Supporting Information

Wylie et al. 10.1073/pnas.1103728108

SI Text

The Chemical Shift Tensor. The electronic environment surrounding the nucleus gives rise to the CST. In the presence of an external magnetic field, B_0, the electrons in the orbitals surrounding these nuclei orient themselves either with the field or against the field, shifting the observed frequency of precession. The chemical shift, δ^{CS}, is typically represented as a Cartesian tensor composed of three orthogonal axes.

$$\delta^{\mathrm{CS}} = \begin{pmatrix} \delta_{11} & \delta_{12} & \delta_{13} \\ \delta_{21} & \delta_{22} & \delta_{23} \\ \delta_{31} & \delta_{32} & \delta_{33} \end{pmatrix} \quad \textbf{[S1]}$$

where δ_{ii} are the nine components of the CST. In solution, isotropic molecular tumbling averages this tensor and the familiar isotropic "chemical shift" (δ_{iso}) is one third the trace of the above tensor:

$$\delta_{\mathrm{iso}} = \frac{1}{3}(\delta_{11} + \delta_{22} + \delta_{33}). \quad \textbf{[S2]}$$

Here, δ_{11} is the most downfield tensor element, δ_{33} the furthest upfield, with δ_{22} between these two extremes. The orientation of these elements to the molecular frame can be described by a series of angles. Often, these are a set of Euler angles in a common coordinate system. In the convention presented, here these angles are defined as α_n, the angle between the nth tensor element and the ^{1}H-^{13}C or ^{15}N-H vector, and β_n, the orientation of the nth tensor element and the ^{13}Cα-^{15}N vector, illustrated in Fig. 1. An alternate description of the CST was popularized by Haeberlen, Merhing, and Waugh. In this convention, very convenient for conversion from a Cartesian to spherical tensor basis set, labels the three axes δ_{xx}, δ_{yy}, δ_{zz}. They are then ordered by their deviation from the isotropic chemical shift, with δ_{zz} having the greatest deviation, followed by δ_{xx} and δ_{yy} closest to the δ_{iso}. In this convention tensor magnitude and rhombicity are defined by two parameters δ (or $\delta_{\mathrm{aniso}} = \delta_{zz} - \delta_{\mathrm{iso}}$) and η ($\eta = (\delta_{xx} - \delta_{yy})/\delta$).

Order Parameters. The experimentally determined ^{1}H-^{15}N and ^{1}H-^{13}C vector orientation report upon both bond distances as well as molecular motion. The assumption is that if the ^{1}H-^{15}N bond length is approximately 1.04 Å and the ^{1}H-^{13}C bond length is approximately 1.12 Å, in the presence of fast rigid motions, the order parameter S is the ratio of the measured dipolar coupling to the ideal dipolar coupling. This approach is the same as that used in recent studies of both ubiquitin (1) and thioredoxin (2). The order parameters for both NH and CH are presented in Fig. S3. The values of S measured from the Hα-Cα dipole (Fig. S3*A*) reveal a rigid backbone, where $S \sim 0.95$ for most sites, comparable to values measured in solid thioredoxin (2) but larger than the S values observed in solid ubiquitin (1). It is known that L12 and G41 in GB1 experience significant motional averaging; however, L12 is not labeled in this sample and the glycine ^{1}H-^{13}C trajectories were not fit because of the high degeneracy of solutions arising from the presence of two directly bound protons; however, the residues adjacent to these sites (T11, K13, D40) do exhibit motional averaging greater than 1 standard deviation from the other sites. Based upon a recent study by Case et al., (3) dipolar averaging of this magnitude would result only a very small motional averaging of the ^{13}C and ^{15}N CSTs. For example, this study revealed that a Lipari–Szabo order parameter, S^2, determined for F52 in GB3 using HN dipolar terms would be 0.897, however when CSA is considered the value rises to 0.975, this is largely attributed to the motion of the lighter proton relative to the heavier peptide backbone. This indicates there is only small motional averaging of CST magnitudes at sites away from the loop containing G41 in GB1 at ambient temperatures. The order parameters measured from the backbone ^{1}H-^{15}N couplings (Fig. S3*B*) follow a nearly identical pattern to that seen in the ^{1}H-^{13}C results. Here, the G41 ^{1}H-^{15}N tensor dipole can be measured, and reveals significant motional averaging, comparable to that reported by Barchi et al. (4). The main differences relative to the ^{1}H-^{13}C scalings are in the turn near A20, and the turn near T49, due most likely to slightly elongated intermolecular and intramolecular hydrogen bonds. However, in the ^{1}H-^{15}N recoupling experiment, A20 is overlapped with N8, and the signal-to-noise ratio at E19 is poor, so this cannot be confirmed. Overall, however, these measurements reveal a relatively rigid, well-ordered backbone.

Data Analysis and Fitting. The data that was acquired resulted in a total of six trajectories for each fit site in the ^{13}C correlation experiments and five trajectories for each set of ^{15}N correlation experiments. During the fitting first the CST magnitudes were fixed (in the case of ^{13}C previously reported values were used). Following this the $R18_1^7$ trajectory was fit for both effective bond length and relaxation. In the next step angles are fit holding all magnitudes and relaxation fixed. In the fourth step all magnitudes, relaxation parameters, and angles are allowed to vary. It was found during this procedure that modeling of cross polarization helped improve the fit quality, especially in the case of ^{1}H-^{13}C trajectories and [^{1}H-^{13}C]:[^{13}C CST] correlation spectra.

While powerful, these experiments possess a few complexities that needed to be addressed. Tensor correlation experiments in SSNMR are most accurate when the correlated vectors are oriented at 30° or less. To partially overcome this shortcoming, each CST orientation was constrained relative to two different vectors, resulting in an improvement in the fit quality for these near orthogonal orientations. Unlike the ^{1}H-^{13}C dipolar tensor, the Cα CST deviates significantly from axial symmetry, and a single correlation of one tensor to another can be ambiguous in isolated regions of conformational space. To address this, we acquired several different ratios of ROCSA to $R18_1^7$ evolution times. This allowed for tighter constraints on the Cα tensor, and also alleviated errors arising from ^{1}H-^{13}C distance measurements. Using this approach we found that varying the ^{1}H-^{13}C dipolar coupling by up to 1 kHz resulted in minimal perturbation (x-y°) in the fitted orientations.

1. Lorieau JL, McDermott AE (2006) Conformational flexibility of a microcrystalline globular protein: Order parameters by solid-state NMR spectroscopy. *J Am Chem Soc* 128:11505–11512.
2. Yang J, Tasayco ML, Polenova T (2009) Dynamics of reassembled thioredoxin studied by magic angle spinning NMR: Snapshots from different time scales. *J Am Chem Soc* 131:13690–13702.
3. Tang S, Case DA (2007) Vibrational averaging of chemical shift anisotropies in model peptides. *J Biomol NMR* 38:255–266.
4. Barchi JJ, Grasberger B, Gronenborn AM, Clore GM (1994) Investigation of the backbone dynamics of the Igg-binding domain of streptococcal protein-G by heteronuclear 2-dimensional ^{1}H-^{15}N nuclear magnetic resonance spectroscopy. *Protein Sci* 3:15–21.

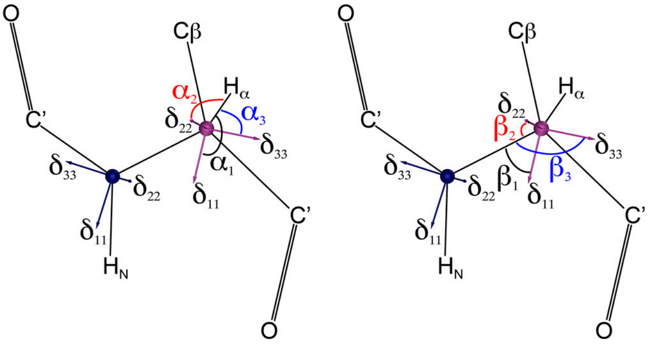

Fig. S1. Orientation of the ^{15}N and $^{13}C\alpha$ chemical shift tensors to the molecular frame. Typically the tensor may be described using sets of angles to orient each tensor element to the molecular bonds. Tensor elements are ordered by furthest downfield (11) to furthest upfield (33). In the text presented here these angles are defined as α_n, the angle between the nth tensor element and the ^1H-^{13}C or ^{15}N dipole, and β_n, the orientation of the nth tensor element to the $^{13}C\alpha$-^{15}N dipole. This convention was used because it was the most convenient to compare measured CST information to ab initio surfaces. Figure was made using SIMMOL package.

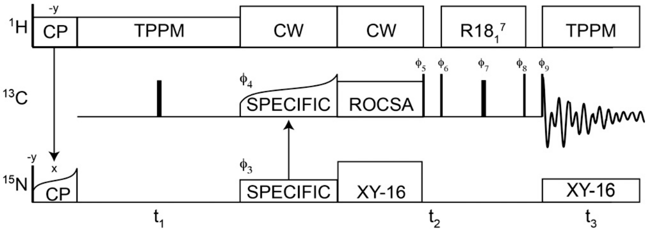

Fig. S2. ROCSA:R1817 CST-dipole correlation sequence. Polarization is created on ^1H and transferred to ^{15}N by adiabatic cross-polarization with a 1-ms contact time. Following a ^{15}N chemical shift evolution period (t_1), polarization is transferred to ^{13}C using SPECIFIC cross polarization. The $^{13}C\alpha$ CST is recoupled under ROCSA followed by a *z*-filter and a synchronously evolved R1817 period that recouples the ^1H-^{13}C dipolar interaction. This is followed by a second *z*-filter and acquisition. Phase cycle is as follows: $\phi_3 = 0, 180, 0, 180, 0, 180, 0, 180$; $\phi_4 = 0, 0, 180, 180, 0, 0, 180, 180$; $\phi_5 = 270, 270, 90, 90, 90, 90, 270, 270$; $\phi_6 = 90, 90, 270, 270, 270, 270, 90, 90$; $\phi_7 = 0, 180, 90, 270, 270, 90, 180, 0$; $\phi_8 = 270, 270, 90, 90$; $\phi_9 = 0, 0, 90, 90, 180, 180, 270, 270$. The following receiver cycle was used: 0, 2, 3, 1, 0, 2, 3, 1, 2, 0, 1, 3, 0, 2, 3, 1.

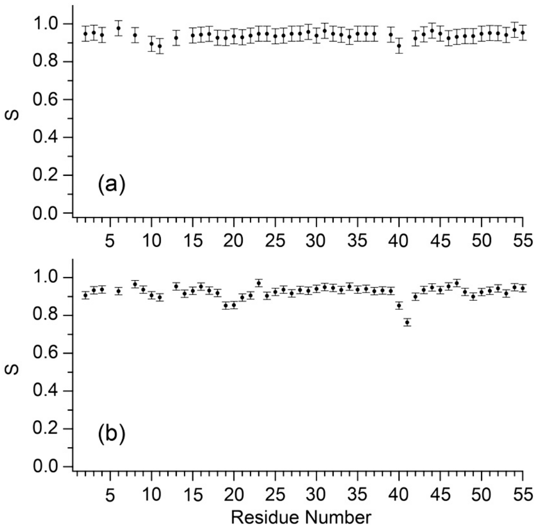

Fig. S3. Order parameters (*S*) measured from backbone ^1H-^{13}C (*A*) and ^1H-^{15}N (*B*) effective dipolar couplings. Equilibrium bond lengths for ^1H-^{13}C and ^1H-^{15}N were assumed to be 1.12 Å and 1.04 Å, respectively. Dipolar interaction was recoupled using $R18_1^7$ pulse sequence element applied at 11.111 kHz spinning (100 kHz B_1 field). ^1H-^{13}C and ^1H-^{15}N couplings were read from the third dimension of a 3D experiment implementing NCA 2D plane to provide site resolution. Data were acquired at VT set temperature of 0 °C and ^1H Larmor frequency of 500 MHz.

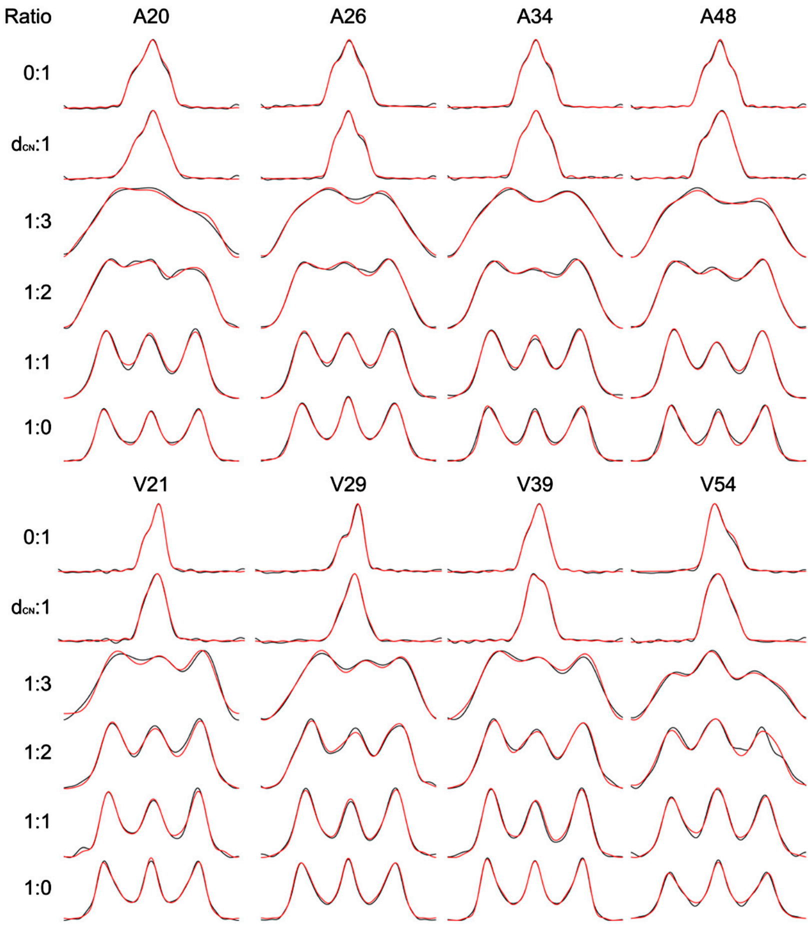

Fig. S4. Analysis of ^{1}H-^{13}C dipole: ^{13}C CST correlation spectra. Fit lineshapes for [^{1}H-^{13}C] : [^{13}C CST] correlation spectra for alanine and valine with different secondary structures are presented. Experimental data are presented in black and best fit are in red. Ratios correspond to ratio of dipolar evolution time to CST evolution time. A20 is located in a turn with β-sheet geometry, A26 and A34 are located in the α-helix, and A48 is in a turn with α-helical geometry. V21 is in a turn with near helical geometry, V29 is in a helix, V39 is in a turn with mixed geometry, and V54 is β-sheet.

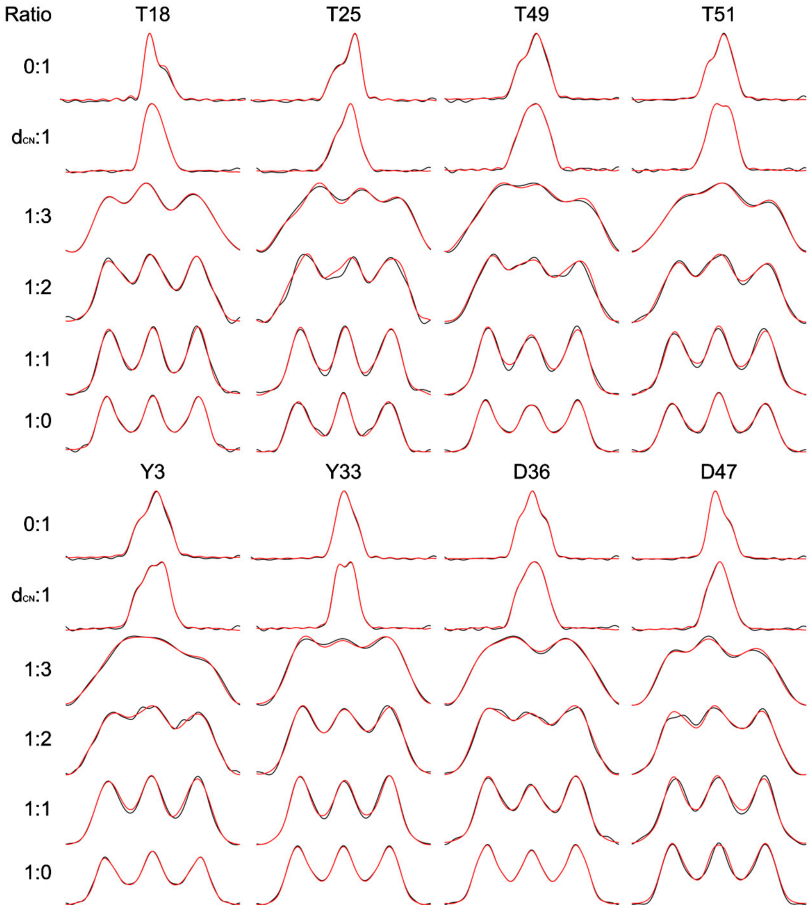

Fig. S5. Analysis of ^{1}H-^{13}C dipole: ^{13}C CST correlation spectra. Fit lineshapes for [^{1}H-^{13}C] : [^{13}C CST] correlation spectra for threonine, tyrosine, and aspartic acid residues with different secondary structures are presented. Experimental data are presented in black and best fit are in red. Ratios correspond to ratio of dipolar evolution time: CST evolution time. In the examples provided, T18 and T51 have β-sheet geometry. T25 is located in the α-helix and T49 is in the turn between β3 and β4. Y3 is β-sheet and Y33 is α-helical. D36 is located at the end of the α-helix and D47 is at the end of β3 leading into a β-turn.

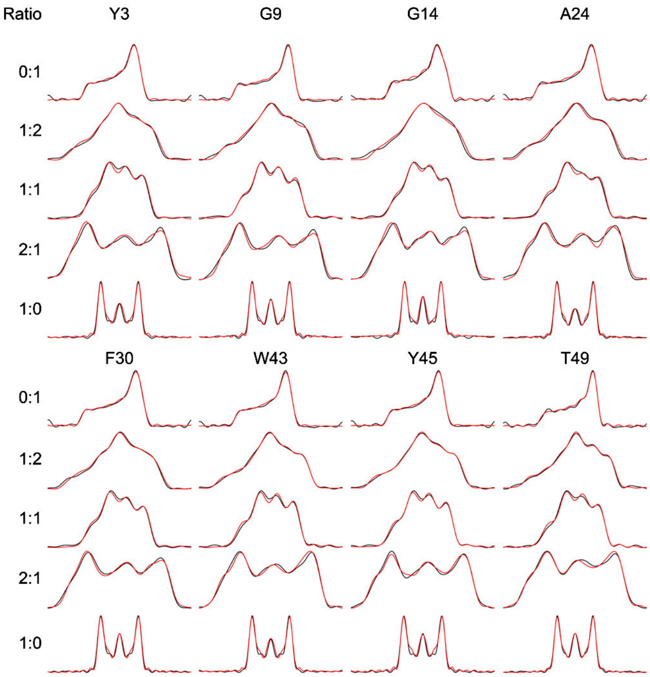

Fig. S6. Amide chemical shift tensor analysis for protein GB1. Fit ensemble of [^{1}H-^{15}N] : [^{15}N CST] correlation spectra. Data is presented in black with best fit in red. The ratio is the ratio of dipolar:CST evolution time for each lineshape. Typical rmsd between theory and experiment is less than 2%.

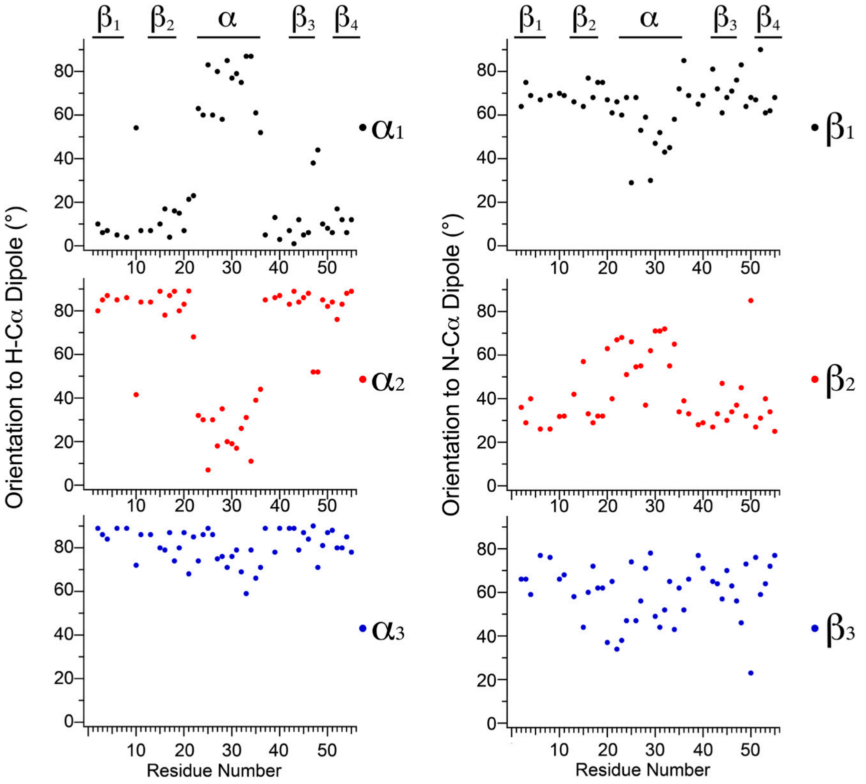

Fig. S7. Expanded view of Fig. 2. Analysis of ^{1}H-^{13}C dipolar:^{13}C CST correlation spectra. In the left column, fit α angles, defining orientation of each tensor element to the HC dipole, as a function of residue number. All angels over 180° were converted to their <90° compliment for clarity. Clear trends are observed where δ_{11} is oriented within 20° of dipole in β-strands but moves within 30° of bond normal in the α-helix. δ_{22} and δ_{33} are near perpendicular to the HC bond in the β-sheet, while δ_{22} reorients up to 80° in the α-helix. In the right column, fit β angles defining the orientation of each tensor element to the NC bond vector. While overall variation of orientation is not as pronounced, there is a strong shift in the β_2 angle between helical and sheet conformations with a concerted, smaller adjustment of β_1 and β_3.

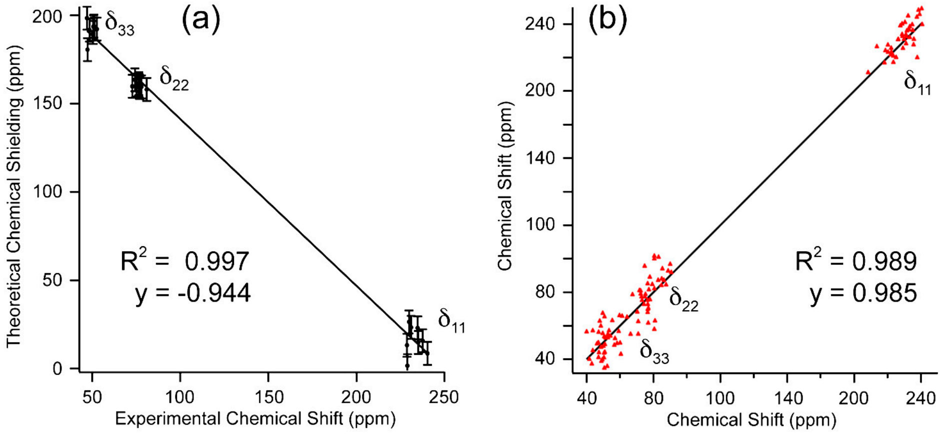

Fig. S8. ^{15}N tensor data compared to solution NMR studies and ab initio calculations. (*A*) Theoretical chemical shielding tensor calculations of helical residues 26–33 in GB3 plotted against measured chemical shift tensor measurements. Calculations presented are from Cai and Fushaman. Overall statistical agreement is good, $R^2 = 0.993$, rmsd = 6.5 ppm. Least squares fit slope of −0.944 with y intercept of 235.7 ppm. Once E27 outlier is removed agreement improves to $R^2 = 0.997$, rmsd = 4.3 ppm, with a least squares slope of −0.938, and y intercept of 236.6 ppm. Statistical agreement is within combined experimental and computational error for all sites but E27. For comparison, the recent solution NMR study of Yao et al. shows $R^2 = 0.986$, rmsd = 9.1 ppm, least squares slope of −0.916, with y intercept of 233.5 ppm. (*B*) Chemical Shift Tensor Principal elements measured by Yao et al. plotted against our measured values. Overall statistical agreement is good when considering the full tensor. Overall rmsd is 8.1 ppm, with R^2 of 0.989 and a slope near unity with y offset of 1.5 ppm.

Table S1. ^{13}C CST orientation to ^{1}H-^{13}C and ^{15}N-^{13}C dipoles

Residue	α_1(± 10°)	α_2(± 10°)	α_3(± 10°)	β_1 (± 15°)	β_2 (± 15°)	β_3 (± 15°)
M1						
Q2	10	100	89	116	36	66
Y3	6	95	94	105	29	114
K4	7	87	96	111	40	121
L5						
I6	175	85	89	67	26	103
L7						
N8	176	86	91	69	26	76
G9						
K10	53	138	73	110	32	66
T11	173	96	86	69	148	112
L12						
K13	7	84	86	114	42	122
G14						
E15	10	89	80	116	57	136
T16	17	102	101	103	147	60
T17	4	87	87	112	151	72
T18	16	91	106	105	148	62
E19	15	100	100	105	32	118
A20	7	97	93	113	117	37
V21	158	91	112	119	40	115
D22	23	68	95	114	67	34
A23	117	148	106	120	68	142
A24	120	150	94	112	51	133
T25	83	173	91	29	66	106
A26	120	150	94	115	55	134
E27	100	162	75	127	55	56
K28	58	145	76	59	37	71
V29	95	160	109	30	62	102
F30	77	161	76	47	71	49
K31	79	163	79	52	71	44
Q32	105	154	69	137	72	52
Y33	93	149	59	45	55	65
A34	87	169	101	122	65	43
N35	119	141	66	108	34	62
D36	128	136	71	95	39	52
N37	175	85	89	69	147	66
G38						
V39	167	86	102	65	28	77
D40	177	87	89	69	29	71
G41						
E42	7	97	89	99	27	65
W43	1	89	89	108	147	64
T44	12	84	101	119	133	57
Y45	175	86	93	68	30	70
D46	6	88	84	109	34	117
D47	142	128	90	104	37	56
A48	136	128	109	83	45	46
T49	170	95	81	64	148	107
K50	172	98	93	68	95	157
T51	6	84	92	113	27	76
F52	17	104	100	90	31	121
T53	12	97	100	119	140	64
V54	6	88	95	118	34	108
T55	12	91	102	112	155	77
E56						

The angles $\alpha_{(11,22,33)}$ define the angle between each tensor element and the ^{1}H-^{13}C dipole. The angles $\beta_{(11,22,33)}$ define the angle between each tensor element and the ^{15}N-^{13}C dipole.

Table S2. ^{15}N CST elements and orientation to ^{1}H-^{15}N dipole

Res.	δ (± 2.5 ppm)	η (± 0.03)	δ_{11} (± 2.5 ppm)	δ_{22} (± 3.0 ppm)	δ_{33} (± 4.0 ppm)	α_1 (± 5°)	α_2 (± 12°)	α_{33} (± 12°)
M1								
Q2	109.0	0.29	234.2	86.7	54.8	18	101	77
Y3	103.0	0.26	226.3	85.4	58.3	18	90	72
K4	106.0	0.25	228.7	82.8	56.6	19	101	80
L5								
I6	104.6	0.28	230.9	88.8	59.2	9	95	82
L7								
N8	92.3	0.24						
G9	108.6	0.22	218.2	67.5	43.1	22	102	73
K10	109.6	0.25	230.7	80.0	52.6	16	98	76
T11	109.7	0.15	216.1	60.0	43.1	17	95	74
L12								
K13	104.4	0.29	227.7	86.2	55.9	16	92	75
G14	105.7	0.32	211.3	69.5	36.0	22	95	69
E15	109.7	0.23	230.8	79.0	53.5	17	93	73
T16	105.0	0.23	220.2	74.9	50.5			
T17	107.0	0.26	223.1	76.5	48.7			
T18	105.8	0.26	222.1	77.3	49.5	16	102	80
E19	103.8	0.32	229.2	90.0	57.0	6	96	88
A20	107.9	0.22	233.8	84.0	60.0			
V21	107.2	0.22	223.5	74.7	50.7	23	92	67
D22	117.5	0.16	233.0	66.3	47.2	24	93	66
A23	112.7	0.25	235.5	80.5	52.3			
A24	114.9	0.25	235.7	77.8	48.9	16	94	74
T25	114.2	0.19	231.6	70.9	49.7	21	105	77
A26	116.3	0.26	240.3	81.0	50.7	16	96	75
E27	112.5	0.23	228.9	72.8	47.4	19	97	73
K28	112.5	0.25	229.9	75.2	47.1	14	95	77
V29	109.4	0.22	228.7	76.5	52.8	14	99	80
F30	112.3	0.25	231.0	76.6	48.5	19	98	73
K31	116.7	0.20	237.5	74.3	50.6	18	98	74
Q32	113.7	0.24	235.0	77.9	51.0	14	93	76
Y33	113.7	0.23	234.7	76.9	51.3	19	98	73
A34	118.0	0.22	240.7	76.5	50.9	21	105	77
N35	113.1	0.20	231.3	73.2	50.1	18	98	74
D36	112.2	0.21	233.3	76.6	53.4	20	97	72
N37	105.3	0.28	220.3	76.9	47.9	22	99	71
G38	116.7	0.17	225.1	60.1	40.0	22	110	81
V39	115.9	0.15	237.7	72.3	55.4	18	98	74
D40	102.6	0.19	233.7	89.3	70.3	13	100	83
G41	84.1	0.30	192.2	78.7	53.4	20	94	71
E42	104.5	0.31	223.5	83.1	50.4	20	100	73
W43	105.4	0.24	230.4	84.9	59.7	20	100	73
T44	104.4	0.29	213.6	72.3	41.7	18	98	74
Y45	103.6	0.24	222.2	79.3	54.3	16	96	75
D46	106.6	0.22	232.9	84.8	61.3	17	103	79
D47	103.0	0.36	226.4	90.6	53.1			
A48	115.7	0.22	234.7	74.1	48.2	18	96	73
T49	104.1	0.16	208.3	60.5	43.7	21	91	69
K50	118.8	0.18	238.5	70.9	49.7	18	99	75
T51	109.9	0.24	221.9	70.3	43.7	20	91	70
F52	108.8	0.21	239.1	87.5	64.2	21	102	73
T53	106.5	0.24	218.7	71.6	46.2	17	100	76
V54	109.2	0.31	227.6	80.5	47.1	20	91	71
T55	109.2	0.31	233.3	86.2	52.8	22	96	69
E56								

The angles $\alpha_{(11,22,33)}$ define the angle between each tensor element and the ^{1}H-^{15}N dipole.

Table S3. Structural quality as assessed by Procheck

Restraints Used							Ramachandran Quality %		X-ray Structure Equivalence			
Structure	T	D	C	O	V	SE	Most Favored	Allowed	Rama	H-bondEnergy	$\chi1$	χ_2
1				X			77.0	22.2	2.5	2.9	1.8	1.0
2		X	X	X			94.0	6.0	1.0	3.3	1.9	1.0
3	X	X					94.0	6.0	1.0	3.4	3.2	1.7
4	X		X	X			86.0	14.0	1.8	2.7	2.3	1.3
5	X	X	X	X			93.8	6.2	1.0	3.0	2.2	1.4
6	X	X	X	X	X		96.0	4.0	1.0	3.0	2.4	1.2
7	X	X			X	X	100.0	0.0	1.0	2.9	2.0	1.0
8	X		X	X	X	X	95.8	4.2	1.0	2.8	1.9	1.0
9	X		X	X		X	93.2	6.8	1.0	2.6	1.9	1.0
10	X	X	X	X		X	96.0	4.0	1.0	2.8	1.8	1.0
11	X	X	X	X	X	X	96.4	3.6	1.0	2.8	1.8	1.0
2QMT							96.0	4.0	1.0	1.5	1.0	2.1
2GI9							94.0	6.0	1.0	1.2	1.0	1.9
1PGA							92.0	8.0	1.0	1.4	1.4	2.1
1PGB							90.0	10.0	1.0	1.0	1.5	2.1
2JSV		X			X		92.0	8.0	1.0	4.0	3.2	1.6

Table S4. Agreement of CST magnitudes and orientations with theory for all structures

							CST		$\alpha_{(1,2,3)}$		$\beta_{(1,2,3)}$	
Structure	T	D	C	O	V	SE	RMSD(ppm)	R^2	RMSD (°)	R^2	RMSD (°)	R^2
1				X			3.6	0.95	4.7	0.99	5.7	0.98
2		X	X	X			2.1	0.98	5.6	0.98	6.6	0.97
3	X	X					3.1	0.96	11.0	0.93	9.6	0.93
4	X		X	X			2.1	0.98	5.5	0.98	6.5	0.97
5	X	X	X	X			2.0	0.98	5.6	0.98	6.6	0.97
6	X	X	X	X	X		2.1	0.98	5.8	0.98	6.7	0.97
7	X	X			X	X	2.9	0.96	9.3	0.96	9.0	0.95
8	X		X	X	X	X	2.1	0.98	5.8	0.98	6.6	0.97
9	X		X	X		X	2.0	0.98	5.7	0.98	6.5	0.97
10	X	X	X	X		X	2.0	0.98	5.6	0.98	6.6	0.97
11	X	X	X	X	X	X	2.1	0.98	5.5	0.98	6.7	0.97
2QMT							2.5	0.97	8.0	0.97	8.5	0.95

Table S5. Agreement of structures with measured pseudodihedral angles

Restraints Used							VEAN		
Structure	T	D	C	O	V	SE	rmsd (°)*	dev. > 5°*	dev. > 10°*
1				X			11.5	40	21
2		X	X	X			7.4	27	12
3	X	X					8.1	41	17
4	X		X	X			9.1	31	16
5	X	X	X	X			6.7	26	11
6	X	X	X	X	X		3.5	11	2
7	X	X			X	X	3.0	12	4
8	X		X	X	X	X	3.0	11	2
9	X		X	X		X	8.6	33	14
10	X	X	X	X		X	8.6	34	14
11	X	X	X	X	X	X	3.0	13	2
2QMT[†]							6.1	28	13

*After accounting for experimental error.

[†] Assuming canonical ^{1}H bond lengths, bond angles, and positions.

Table S6. Agreement of experimental isotropic chemical shifts with shifts predicted by SPARTA for each structure

								Cα		Cβ		C′	
Structure	N	T	D	C	O	V	SE	RMSD (ppm)	R^2	RMSD (°)	R^2	RMSD (°)	R^2
1	X				X			1.08	0.95	1.35	0.99	1.23	0.8
2	X		X	X	X			1.06	0.95	1.28	0.99	1.15	0.8
3	X	X	X					1.04	0.96	1.25	0.99	1.14	0.8
4	X	X		X	X			1.01	0.96	1.13	0.99	1.13	0.8
5	X	X	X	X	X			1.02	0.96	1.13	0.99	1.16	0.8
6	X	X	X	X	X	X		1.04	0.96	1.15	0.99	1.19	0.8
7	X	X	X			X	X	1.04	0.96	1.27	0.99	1.16	0.8
8	X	X		X	X	X	X	1.01	0.96	1.13	0.99	1.13	0.8
9	X	X		X	X		X	1.01	0.96	1.13	0.99	1.13	0.8
10	X	X	X	X	X		X	1.01	0.96	1.13	0.99	1.13	0.8
11	X	X	X	X	X	X	X	1.03	0.96	1.14	0.99	1.14	0.8
2QMT								0.93	0.97	0.99	0.99	1.12	0.8

Table S7. Backbone rmsd among crystal structures and SSNMR structure

Structure	SSNMR	2QMT	2GI9	1PGA	1PGB	Crystal Avg.
SSNMR	—	0.51	0.58	0.54	0.53	0.54
2QMT	0.51	—	0.47	0.39	0.28	0.39
2GI9	0.58	0.47	—	0.24	0.36	0.37
1PGA	0.54	0.39	0.24	—	0.25	0.30
1PGB	0.53	0.28	0.36	0.25	—	0.30
Crystal Avg	0.54	0.39	0.37	0.30	0.30	—

Table S8. Table of TALOS restraints that violated at some point during annealing and refinement

Residue	Angle	TALOS Prediction (°)	Doubled TALOS error (°)
Q2	ϕ	−109	34.0
N8	ϕ	−100	34.0
T11	ϕ	−94.0	34.0
E19	ϕ	−117.0	20.0
A24	ϕ	−65.0	24.0
E27	ϕ	−66.0	16.0
N37	ϕ	−105.0	32.0
V39	ϕ	−101.0	30.0
W43	ϕ	−122.0	32.0
T49	ϕ	−110.0	36.0
T11	ψ	−6.0	28.0
T18	ψ	137.0	28.0
A26	ψ	−41.0	10.0
Y33	ψ	−37.0	18.0
D36	ψ	−31.0	16.0
W43	ψ	160.0	20.0
Y45	ψ	126.0	48.0
T49	ψ	10.0	26.0
T51	ψ	134.0	32.0
T53	ψ	144.0	34.0

Table S9. Distances lengthened during structure calculations

Residue	Resonance	Residue	Resonance	Distance	Low error	Upper Error
A23	CB	Y3	CZ	2.75	1.75	3.00
I6	CG1	T53	CB	3.05	2.05	3.05
M1	CE	E19	CG	3.55	2.55	3.55
Q2	CD	K50	CA	4.25	3.25	5.00
I6	CG1	T53	CB	3.55	2.55	3.55
T18	C	Y3	CZ	4.25	3.25	4.25
Y33	C	L7	CD(1,2)	3.55	2.55	4.55
I6	CG1	T53	CB	3.70	2.70	3.70
T53	CB	L7	CD(1,2)	3.70	2.70	5.00
Y33	C	L7	CD(1,2)	3.83	2.83	4.00
N8	CA	L12	CG	4.25	3.25	4.25
E42	HN	V54	HN	4.75	3.75	5.75
V54	HN	E42	HN	3.25	2.25	3.25
A26	N	A20	CB	4.43	1.00	1.00
F30	N	Y33	CB	3.82	0.28	1.28
G38	N	L12	CD1	4.31	2.00	2.00
N37	ND2	L12	CD1	3.06	1.00	1.00
E15	N	L7	CD2	4.76	1.00	1.00
K13	N	L7	CD2	4.79	1.00	1.00
K13	NZ	L7	CD2	6.73	1.00	1.00
A23	N	M1	CE	4.20	1.04	2.10
M1	N	M1	CE	3.77	1.60	1.60
K31	N	E27	CG	4.19	1.60	2.60
K28	N	K28	CG	2.67	1.22	1.22
Q2	N	M1	CG	3.01	1.00	1.00
F30	N	V29	CG1	2.81	1.00	1.00
N37	N	V39	CG1	5.64	1.39	1.39
Q32	N	V54	CG1	4.50	3.50	4.50
G41	N	V54	CG2	3.05	0.10	1.00
T18	N	E19	CD	6.86	0.35	1.35
G9	N	K13	CE	3.65	1.38	1.38
T11	N	K13	CE	4.36	0.67	1.67
T44	N	W43	CZ3	5.04	0.43	1.43
Q2	N	M1	CG	2.86	1.00	1.00
T17	N	T16	CG2	3.90	1.10	1.10
E19	N	T17	CG2	5.45	1.00	2.00
W43	N	T55	CG2	5.72	1.10	2.10
G41	N	V54	CG2	2.93	0.10	1.00
N37	N	Y33	CG	5.27	1.00	1.00